Dual-Band Bandpass Coaxial Cavity Filters With Controllable Center Frequencies and Bandwidths Using F-Shaped Resonators

WENHAO LI [1], **YUN LIU** [1] **(Member, IEEE), AND SHANHUI PEI** [2]

(Regular Paper)

[1]College of Electronic and Information Engineering, Nanjing University of Aeronautics and Astronautics, Nanjing 210016, China
[2]The 43rd Research Institute of China Electronics Technology Group Corporation, Hefei 230088, China

CORRESPONDING AUTHOR: Yun Liu (e-mail: lycloud1978@163.com).

ABSTRACT   In this study, a novel dual-band bandpass coaxial cavity filter with large design freedoms for center frequencies and bandwidths is proposed by introducing F-shaped dual-mode resonators. Each F-shaped dual-mode resonator is capacitively loaded with two tuning screws for simultaneously tuning two frequencies. A dual-iris structure is implemented for the couplings between the two dual-mode resonators, with two screws applied to enhance the couplings. A dual-disc capacitive coupling is implemented at the input and output ports. By introducing these structures, the frequencies and bandwidths of the two passbands can have large design freedoms. A third-order dual-band filter at 0.845 GHz/1.790 GHz with bandwidths of 12 MHz/26 MHz is also designed, fabricated, and measured. Low insertion losses of 0.4 dB and 0.35 dB are achieved at the passbands. In comparison with planar dual-band bandpass filters, the filter presented in this study offers lower insertion losses and more convenience in filter tuning.

INDEX TERMS   Cavity filter, dual-band bandpass filter, F-shaped dual-mode resonator.

I. INTRODUCTION

Recently, the increasing demand for wireless communication has increased the requirement for dual-mode or multimode transceivers or systems that can support two or more communication standards. Consequently, dual-band bandpass filters have attracted the attention of many researchers.

Industrial dual-band bandpass filters are always realized by two filters that share the same input and output ports [1], but they entail complex structures and large dimensions. Dual-mode resonators, such as stepped-impedance resonators [2] and stub-loaded resonators (SLRs) [3] in planar forms, are used to construct dual-band filters, but the bandwidths can hardly be independently assigned due to limited design freedoms. Microstrip and defected ground structure resonators implemented on two layers of a substrate can also be used to realize two passbands, but their development is costly [4].

In contrast to planar dual-band filters, cavity-type dual-band bandpass filters offer considerably lower insertion loss. In [5], a dual-capacitively loaded waveguide cavity resonator is proposed for the dual-band filter, but bandwidths cannot be designed independently. In [6], a triple-conductor TEM dual-mode resonator is proposed, and a dual-band bandpass filter is designed with good features (i.e., low insertion loss). In [7], a dual-band bandpass filter is implemented within a waveguide, but high insertion loss is obtained because of the high-loss strip-line resonating modes. A low-loss dielectric loaded cavity dual-band bandpass filter with multiple transmission zeros is previously realized by using degenerate TM modes and by introducing nonresonant modes [8]. Double-ground-plane dual-mode coaxial resonators [9] are used to design dual-band bandpass filters with independently tunable frequencies, but the configuration is attained at the expense of a complex structure. Stepped-impedance resonators [10] and SLRs [11] in coaxial form are also used to design dual-band bandpass filters. In [12], a dual-coaxial resonator is proposed to design compact multichannel bandpass filters. In [13], a new class of compact inline dual-band bandpass filters using TM-mode dielectric resonators in planar configuration is
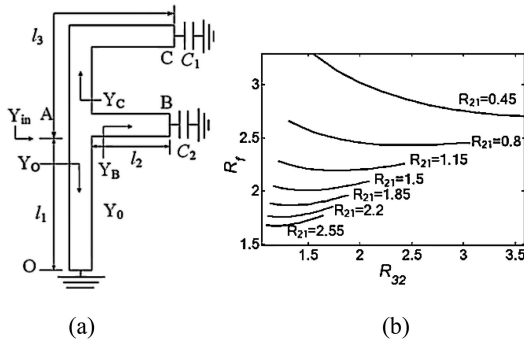
FIGURE 1. F-shaped capacitively loaded dual-mode resonator. (a) F-shaped resonator; (b) R_f versus R_{21} and R_{32}. $R_f = f_2/f_1$; $R_{21} = l_2/l_1$; $R_{32} = l_3/l_2$.

proposed, but frequencies cannot be designed independently. In [14], a dual-band bandpass filter is achieved using close dual post configurations that can generate different resonances. A side-coupled configuration is proposed and implemented in an elliptical waveguide dual-band filter [15]. In [16], a dual-band filter is proposed, and each individual band is controlled by a dedicated polarization of the dual-mode resonators.

Reconfigurable filters have reconfigurable passbands because of the use of varactors [17] or switches [18], and they can be used in dual-mode or multimode telecommunication systems. However, these filters cannot simultaneously work for two or more passbands and have considerably higher insertion loss due to the introduction of high-loss tuning/switching elements.

In this study, the proposed F-shaped dual-mode resonator is used to simplify the structures and ensure flexibility in assigning bandwidths. A dual-iris coupling structure and a dual-disc capacitive coupling structure are adopted in the dual-band bandpass filter design to simultaneously control the two bandwidths. The designed filter exhibits lower insertion losses compared with planar dual-band bandpass filters.

II. F-SHAPED DUAL-MODE RESONATOR AND FILTER DESIGN METHOD

Fig. 1(a) shows the circuit of an F-shaped dual-mode resonator with three sections of transmission lines (i.e., AO, AB, and AC) and is short-circuited at O. Two capacitive loadings C_1 and C_2 are introduced by inserting metal tuning screws. The characteristic admittance of the sections is represented by Y_0. Assuming a pathway from Point A toward three sections, when the values of C_1 and C_2 are sufficiently small to be ignored, the input admittance values can be expressed as follows:

$$Y_O = -jY_0 \cot\left(\frac{2\pi f l_1}{c}\right)$$

$$Y_B = jY_0 \tan\left(\frac{2\pi f l_2}{c}\right)$$

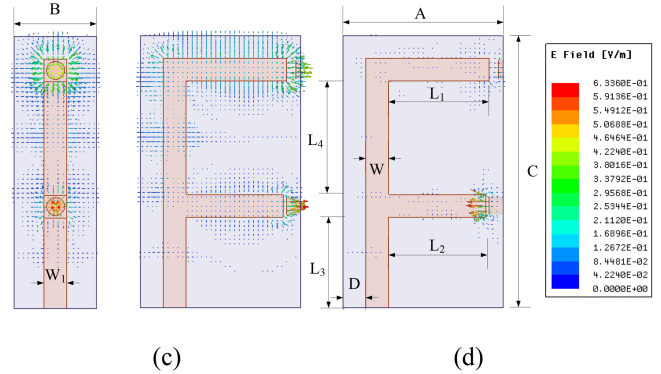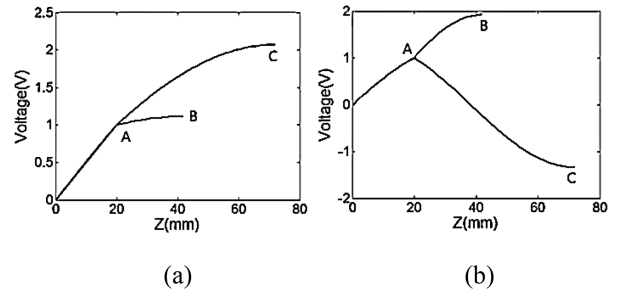$$Y_C = jY_0 \tan\left(\frac{2\pi f l_3}{c}\right). \quad (1)$$

FIGURE 2. Voltage and electric field distributions of two modes: (a) Voltage distribution of mode 1; (b) voltage distribution of mode 2; (c) e-field distribution of mode 1; (d) e-field distribution of mode 2.

Resonance can be achieved by calculating for $Y_{in} = Y_O + Y_B + Y_C = 0$, and the following equation can be obtained after simplification:

$$\tan\left(\frac{2\pi f l_2}{c}\right) + \tan\left(\frac{2\pi f l_3}{c}\right) - \cot\left(\frac{2\pi f l_1}{c}\right) = 0. \quad (2)$$

The transcendental equation can be solved by numerical methods, such as the bisection method. The lowest two zeros are taken as the resonating frequencies of the first and second modes.

The ratio of the center frequency f_2 of the higher frequency to the center frequency f_1 of the lower frequency in the two passbands is defined as R_f, where $R_f = f_2/f_1$. The length ratios of the branches in the F-shaped resonators are defined as R_{21} and R_{32}, where $R_{21} = l_2/l_1$, and $R_{32} = l_3/l_2$. R_f is determined by R_{21} and R_{32}, as shown in Fig. 1(b). By changing the values of R_{21} and R_{32}, R_f can reach a value range of 1.7–3.3. The value range can be expanded by setting larger value ranges for R_{21} and R_{32}.

With a fixed value of R_f, the resonant frequencies f_1 and f_2 are inversely proportional to the section lengths of an F-shaped resonator. Moreover, by tuning the values of R_{21} and R_{32}, the frequency ratio R_f can be efficiently adjusted, as shown in Fig. 1(b). Thus, the central frequencies of the two passbands can be freely adjusted by changing the three section lengths of the resonator. In practical design, the eigenmode solver of the commercial software HFSS [19] can be used to simulate the resonator precisely.

Fig. 2(a) and (b) show the voltage distributions of the two resonating modes when $l_1 = 20$ mm, $l_2 = 22$ mm, and $l_3 =$
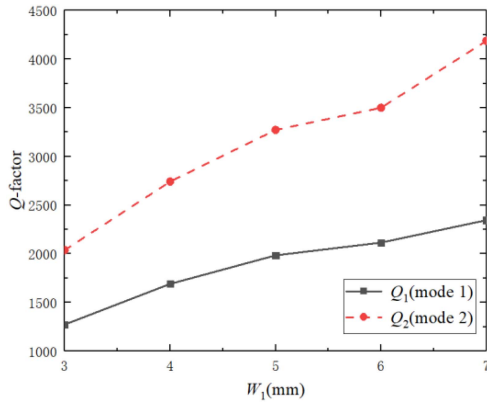
FIGURE 3. Effect of resonator width on Q-factor Q_1 and Q_2.

52 mm. Z represents the length between Point O and other points in the F-shaped dual-mode resonator. The values on the vertical axis reflect the voltage at each place relative to Point O (using the voltage of Point O as the zero potential reference). Furthermore, the maximum voltage for Mode 1 is located at Position C, whereas the maximum voltage for Mode 2 is located at Position B. As demonstrated in Fig. 2(c) and (d), the voltage distributions match the simulated electric distributions of the two resonating modes.

The simulated Q-factor for Mode 1 is $Q_1 = 1984.86$, and the Q-factor for Mode 2 is $Q_2 = 3272.74$. The values of the Q-factor can be achieved using the eigenmode solver of the HFSS. Fig. 3 shows the variations in Q_1 and Q_2 with changing resonator width W_1. The values of the resonant cavity width B and the resonator thickness W in Fig. 2(c) and (d) are also changed simultaneously with the relationships of $W = W_1$ and $B = 3.6 W_1$. Q_1 and Q_2 increase with increased W_1.

Resonators can be coupled in two ways: capacitive and inductive coupling. Capacitive coupling generally occurs in parts with strong electric fields (i.e., here, the electric field is strong at Points C and B of the F-shaped resonators). Inductive coupling occurs in parts with strong magnetic fields. Electric and magnetic field coupling jointly affect the total coupling coefficient.

According to the voltage and electric field distributions of the two modes, the capacitive loading C_1 at Position C can effectively tune the frequency of Mode 1, whereas C_2 at Position B can better tune the second resonating frequency. A combination of C_1 and C_2 is introduced by two screws, which are represented by T_1 and T_2 in Fig. 4(a). These screws can provide full tuning of the two resonating frequencies.

Fig. 4(a) shows the proposed dual-iris coupling structure. Two screws are inserted into the two irises to enhance the coupling between two F-shaped dual-mode resonators. The values of the frequencies of the two modes used in the resonator are 0.845 GHz and 1.790 GHz. Screw S_1 (between Lines AC) introduces more coupling for the lower modes, whereas screw S_2 (between Lines AB) has more effect on Mode 2 coupling. By adjusting the dimension of the two screws, the coupling ratio between the two modes can be effectively tuned.
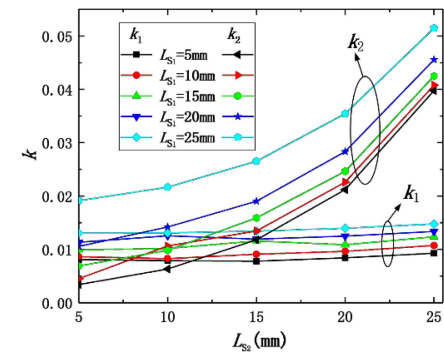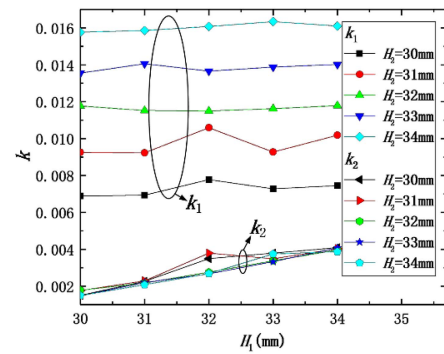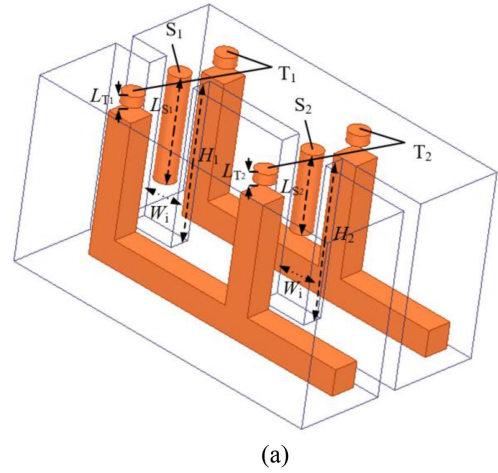

(a)

(b)

(c)

FIGURE 4. Curves of coupling coefficients k_1 and k_2: (a) Dual-iris coupling structure; (b) effects of iris heights on k_1 and k_2 ($L_{S1} = 0.1$ mm, $L_{S2} = 0.1$ mm); (c) effects of screw lengths on k_1 and k_2 ($H_1 = 30$ mm, $H_2 = 30$ mm).

Fig. 4(a) presents a coupled resonator model that uses two F-shaped dual-mode resonators rather than a complete filter. By using this model, coupling coefficients k_1 and k_2 between the two resonators can be calculated. The calculation formula of the coupling coefficient is expressed as follows:

$$k_i = \frac{f_{ei}^2 - f_{oi}^2}{f_{ei}^2 + f_{oi}^2} \quad i = 1, 2, \tag{3}$$

where fe_1, fe_2, fo_1, and fo_2, which represent the even and odd modes of the coupled resonators in Fig. 4(a), can be calculated using the eigenmode solver of the HFSS.

In a third-order filter with a symmetrical structure, the third resonator is symmetrical and the same as the first resonator; thus, its parameters are also the same as the first resonator.

Fig. 4(b) and (c) show many curves of k_1 and k_2, allowing for the viewing of important dimensions, including the heights of the irises H_1 and H_2 and the lengths of the tuning screws L_{S1} and L_{S2}. Among these parameters, L_{S1} and H_2 have larger effects on k_1 and k_2.

Fig. 4(b) also shows that k_1 and k_2 increase with the heights of irises H_1 and H_2. H_2 has a larger effect on coupling coefficient k_1, whereas H_1 has a larger effect on coupling coefficient k_2. Furthermore, Fig. 4(c) shows that the tuning screws loaded in the irises can effectively increase the coupling coefficients. By increasing L_{S1}, both coupling coefficients are effectively increased. If L_{S2} increases, then k_1 remains almost unchanged, whereas k_2 effectively increases. The ratio between k_1 and k_2 can be updated by tuning the four dimensions. Tuning the widths of the irises is expected to have a similar effect as tuning the iris heights.

Fig. 5(a) shows the proposed dual-disc capacitive coupling structure used for input/output coupling. Two capacitive discs are loaded at Positions C and B of the input or output resonator. The discs mainly affect the external Q factor of Modes 1 and 2, with C and B corresponding to the maximum voltage points of each mode. By tuning the disc diameters or the spaces between the discs and the resonator rods, external quality factors Q_{e1} and Q_{e2}, which represent the external couplings, can be tuned.

Fig. 5(b) and (c) show the variations in Q_{e1} and Q_{e2} with changing D_1 and D_2. Q_{e1} is higher when either D_1 or D_2 increases due to decreased capacitive couplings at Position B or C. By contrast, Q_{e2} is higher when D_2 increases and lower when D_1 increases. This finding is due to the fact that the voltage at Point C is inverse to the voltage at Point B for Mode 2, as shown in Fig. 2(c) and (d).

The necessary coupling coefficient k and external quality factor Q_e in the two passbands must be obtained to achieve the required BW$_1$ and BW$_2$, respectively. Coupling coefficient k and the external quality factor Q_e can be calculated as follows:

$$k = \frac{BW/f_0}{\sqrt{g_1 g_2}}, \tag{4}$$

$$Q_e = \frac{g_0 g_1}{BW/f_0}. \tag{5}$$

The realized relative bandwidths of the two passbands are proportional to k_1 and k_2 and inversely proportional to Q_{e1} and Q_{e2}, respectively.

The values of k_1 and k_2 are mostly affected by iris heights (H_1 and H_2) and screw lengths (L_{S1} and L_{S2}). Fig. 4(b) and (c) show the adjustable ranges of k_1 and k_2 by changing the iris heights and screw lengths, which are 0.007–0.016 and 0.001–0.05, respectively. If only one bandwidth is controlled
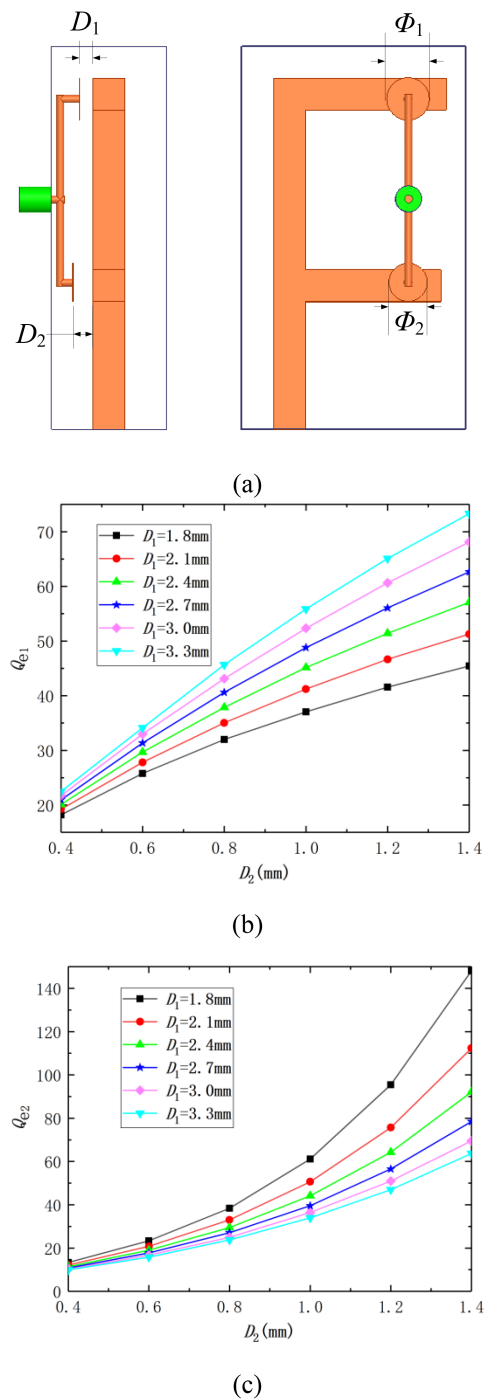

(a)

(b)

(c)

FIGURE 5. Effect of distance between the capacitor disc and resonator on external *Q* factors *Q*$_{e1}$ and *Q*$_{e2}$: (a) Input/output coupling structure; (b) effect on *Q*$_{e1}$; (c) effect on *Q*$_{e2}$.

and the center frequencies of the two passbands are 845 MHz and 1790 MHz, then the value of BW$_1$ can range from 5.25 MHz to 12 MHz with a relative bandwidth of 0.62%–1.42%, and the value of BW$_2$ can range from 1.58 MHz to 79.27 MHz, with a relative bandwidth of 0.088%–4.43%, using (4).

The distances between the capacitive discs and the resonators (D_1 and D_2) are the most influential parameters in
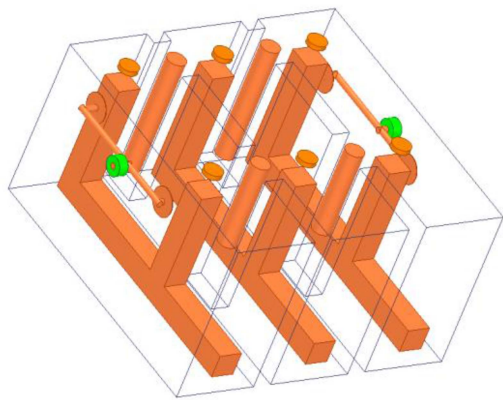
FIGURE 6. Model of the designed third-order filter.

Q_e. The adjustable ranges of Q_{e1} and Q_{e2} shown in Fig. 5(b) and (c) can be obtained by changing D_1 and D_2, which are 17–74 and 10–144, respectively. When only one passband is controlled, the value of BW_1 can range from 8.82 MHz to 38.41 MHz, with a relative bandwidth of 1.04%–4.55%, and the value of BW_2 can range from 9.61 MHz to 138.32 MHz, with a relative bandwidth of 0.54%–7.73%, using (5).

The relative values of k_1 and k_2 can also be adjusted. When H_1 is fixed, as illustrated in Fig. 4(b), by altering H_2, k_1 can be made to be significantly larger than k_2 at specific screw lengths L_{S1} and L_{S2}. Thus, the k_1/k_2 ratio can shift dramatically, with a range of 4–7 (0.016/0.004–0.007/0.001). Similarly, as illustrated in Fig. 4(c), when L_{S1} is fixed, k_2 can be configured to be significantly larger than k_1 at certain iris heights H_1 and H_2. The range of k_1/k_2 ratio is 1.75–3.57 (0.007/0.004 - 0.05/0.014). Hence, the bandwidth ratio of the two passbands can also be adjusted.

Similarly, the relative values of Q_{e1} and Q_{e2} can also be changed. Q_{e1} increases when either D_1 or D_2 increases, but Q_{e2} increases when D_2 grows and decreases when D_1 increases. By adjusting the values of D_1 and D_2, the Q_{e2}/Q_{e1} ratio can be drastically shifted, with a range of 0.59–1.95 (10/17–144/74), implying that the bandwidth ratio of the two passbands can also be adjusted.

By adjusting the values of k_1 and k_2 and Q_{e1} and Q_{e2}, the designed filter can adjust the ranges and ratios of the two passbands over a wide range.

The model of the designed third-order filter is shown in Fig. 6.

III. EXAMPLE FILTER DESIGN AND RESULTS

The 4G network is still used widely at present. The two frequency bands commonly used for mobile phones by China's four major telecom operators are 703–960 MHz and 1710–1880 MHz. Thus, a third-order dual-band bandpass filter is designed with center frequencies of $f_1 = 845$ MHz and $f_2 = 1790$ MHz. The designed bandwidths are $BW_1 = 12$ MHz and $BW_2 = 26$ MHz. The resonators, tuning screws, and capacitive discs are made of copper with a conductivity of 5.7×10^7

S/m. The cavity is made of aluminum with a conductivity of 3.5×10^7 S/m. The cavity and all components are silver-plated to increase the external Q factor of the resonators. For the two passbands, the coupling coefficients and external Q factors at a passband ripple of 0.027 dB can be formulated as

$$Q_{eS}^1 = Q_{eL}^1 = 54.42; \quad k_{12}^1 = k_{23}^1 = 0.016$$
$$Q_{eS}^2 = Q_{eL}^2 = 53.2; \quad k_{12}^2 = k_{23}^2 = 0.0164. \qquad (6)$$

The size of the F-shaped dual-mode resonator is roughly equivalent to the size of the single-mode resonator with the same resonant frequency as the lower resonant frequency of the F-shaped resonator. The resonator dimensions in the aforementioned design are as follows: resonator width $W_1 = 5$ mm, thickness $W = 5$ mm, AO section length $L_3 = 20$ mm, AB section length $L_2 = 21.2$ mm, AC section length $L_4 = 25$ mm, and $L_1 = 22$ mm. The lengths of T_1 and T_2 are $L_{T1} = 1$ mm and $L_{T2} = 3.8$ mm, respectively.

In the dual-iris coupling structure, the width of the two coupling windows is $W_i = 9.8$ mm, and the heights are $H_1 = 24$ mm and $H_2 = 33$ mm. The lengths of the two screws are $L_{S1} = 23$ mm and $L_{S2} = 8$ mm. When the dimensions are determined, the F-shaped resonators and housing are machined separately, and a screw hole is reserved at Point O of each resonator. Then, three F-shaped resonators are mounted to the housing by three screws.

For the dimensions of the input and output structures, the diameters of the two capacitive discs are $\Phi_1 = \Phi_2 = 6.7$ mm, and the distances from Positions C and B of the input or output resonator are $D_1 = 2.65$ mm and $D_2 = 1.15$ mm. In practical implementation, suitable assembly fixtures may be used to ensure good assembly precision. For example, Teflon rods with heights of D_1 and D_2 may be manufactured and placed between the discs and the resonators when fixing the discs to achieve precise distances D_1 and D_2. Nonetheless, the filter must be fine-tuned to achieve good filtering performance. D_1 and D_2 can be changed in actual tuning by varying the bending of the metal lines linked between the SMA connectors and the capacitive discs.

Fig. 7 shows the simulation and measured results of the dual-band bandpass filter. According to the measurement results, the center frequencies of the first and second passbands are 844 MHz and 1794 MHz, with bandwidths of 10 MHz and 24 MHz, respectively. The return loss of both passbands is lower than −20 dB, and the insertion loss values are approximately 0.4 dB and 0.35 dB. A high isolation of 55 dB is achieved between the two passbands. The simulated and measured S-parameters are in good agreement with each other. By using the measured insertion losses, bandwidths, and return losses, the actual Q-factor values of the two modes can be approximated as 2150 for Mode 1 and 3000 for Mode 2. The simulated and calculated approximate actual values of Q-factor are relatively close. The errors between them may be due to ignoring the thickness of the housing, tuning screws, and other practical factors. Fig. 7(d) shows the measured out-of-band response of the designed filter. The first spurious band

(a)

(b)

(c)
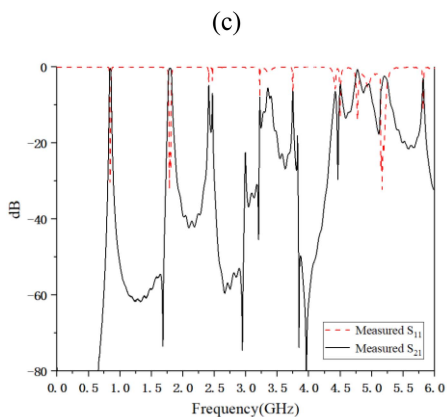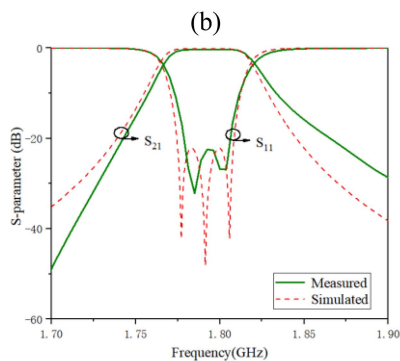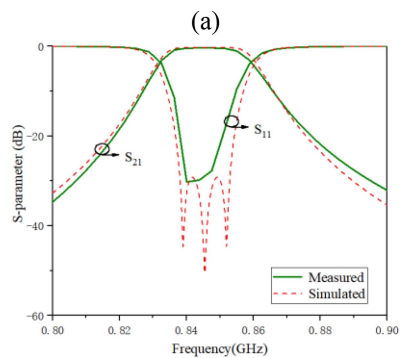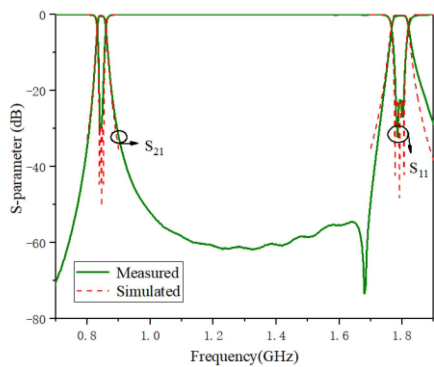
(d)

FIGURE 7. Simulated and measured responses: (a) Response of the wideband; (b) response of the first passband; (c) response of the second passband; (d) response of out-of-band.

FIGURE 8. Photograph of the fabricated dual-band bandpass filter.
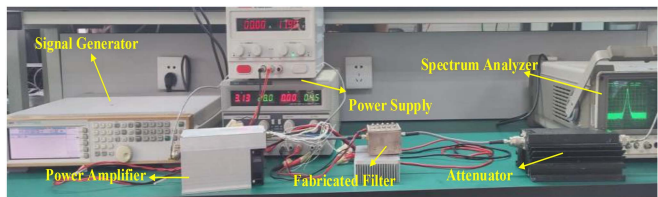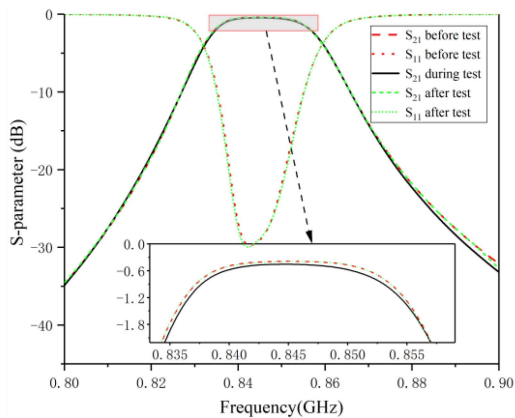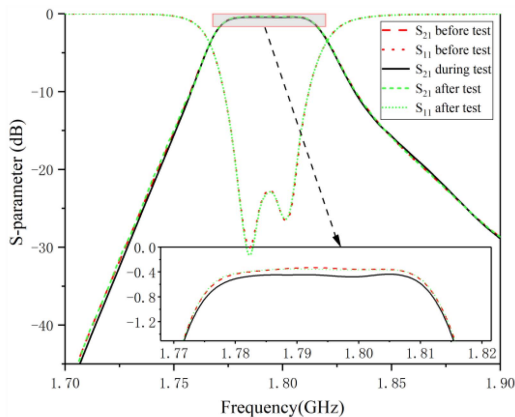

FIGURE 9. Photograph of the power handling testing system.

(a)

(b)

FIGURE 10. S-parameter responses before, during, and after the power handling test: (a) Responses of the lower passband; (b) responses of the higher passband.

TABLE 1. Comparison of the Proposed Filter With Other Filters

	Type	Central frequencies (GHz)	FBW	Insertion loss (dB)	Order	Design freedoms for Freqs and BWs	Size (length * width * height) (λ_g^2/λ_g^3)
[3]	Planar	1.68/2.81	9.4%/7.5%	0.9/1.1	2/2	Small	0.127 × 0.063
		1.83/2.94	8.1%/6.8%	1.7/1.6	2/2	Small	0.195 × 0.068
[4]	Planar	1.55/2.68	N/A	N/A	2/2	Small	0.078 × 0.078
[5]	Cavity	2.4/5.0	1%/1%	1.47/1.01	2/2	Small	1.017 × 0.407 × 0.346
[6]	Cavity	1.88/2.185	4%/2.7%	0.5/0.6	3/3	Large	N/A
[9]	Cavity	2.655/3.550	3.8%/3.1%	0.34/0.39	2/2	Large	0.576 × 0.576 × 0.213
[10]	Cavity	1.2/5.8	3.7%/1.7%	0.43/0.40	2/2	Small	0.07 × 0.07 × 0.24
	Cavity	1/4	19%/20%	0.39/0.16	2/2	Small	0.03 × 0.05 × 0.23
[11]	Cavity	0.9/1.8	31%/15.6%	0.22/0.25	4/4	Large	0.486 × 0.150 × 0.201
[12]	Cavity	2.7/3.1	4.1%/3.1%	0.32/0.41	2/2	Large	0.34 × 0.16 × 0.25
[13]	Cavity	4.86/5.3	1.1%/1.46%	1.1/0.9	3/3	Small	N/A
[14]	Cavity	2.3615/2.7125	2.7%/1.07%	N/A	4/4	Small	N/A
[15]	Cavity	3.435/3.565	1.05%/1%	0.55/0.65	4/4	Small	N/A
[16]	Cavity	11.75/12.25	0.9%/0.9%	N/A	3/3	Large	0.576 × 0.576 × 0.213
This work	Cavity	0.845/1.790	1.4%/1.3%	0.4/0.35	3/3	Large	0.204 × 0.197 × 0.142

*λ_g is the wavelength at the lower operation frequency.

is observed around 2.4 GHz. Fig. 8 presents an image of the fabricated dual-band bandpass filter with a total dimension of 72.5 mm × 70 mm × 50.5 mm.

There are some techniques that can be used to widen the upper stopband and suppress the first spurious band. The simplest method is to employ a lowpass filter, which is often with low loss and is small in dimension. In a second approach, mixed F-shaped resonators [20] may be used. These resonators may have identical first and second resonating frequencies but vastly different third resonating frequencies. The third resonating frequencies cannot be combined to produce the first spurious band. The lengths and widths of the three transmission line sections in Fig. 1(a) may vary among the three F-shape resonators. For the purpose of suppressing the first spurious band, open stubs at the input and output ports are another option.

Errors are expected to arise during processing and manufacturing, further suggesting that the actual situation will also likely differ from the ideal situation. The fabricated filter should be adjusted according to the parameter values obtained from the simulation. Updating can be achieved by continuously adjusting the tuning screws and the capacitor discs at both ends.

Fig. 9 shows the complete power handling testing system. This system consists of two power supplies, a signal generator, a power amplifier (PA), the fabricated filter, an attenuator, and a spectrum analyzer. The power amplifier can work at 0.7–2 GHz, with a maximum output power of 100 W. The result shows that the designed filter can work well at two center frequencies with power of 100 W, proving that the filter can be used in many communication systems.

The filter's contrasted S-parameter responses before, during, and after the power handling test are shown in Fig. 10. Due to the high output power of the PA, calibration on the output port is not possible when measuring the filter during the power handling. Therefore, we determined the gains of the PA (G_1(dB)) and the cascaded PA and filter circuits (G_2(dB)).

S_{21}(dB) of the filter can be roughly calculated as G_2 - G_1 at the two passbands. S_{11} is not provided due to calibration issues. The S-parameter responses measured before and after the power handling test are shown to be in strict agreement in Fig. 10. S_{21}, which was measured during the power handling test, almost has the same curve as the other plots, but because of a lack of calibration, it has a slightly different passband insertion loss.

Table I presents a comparison between the proposed filter and other reported planar and cavity filters. Similar to other cavity filters, the proposed filter has considerably lower insertion loss than planar dual-band bandpass filters, because of the markedly higher quality factor of the cavity resonators. The filters in [10] use stepped impedance resonators to achieve dual-narrowband and dual-wideband filters, but it lacks the elements in this study that can improve the ability to control the center frequencies and bandwidths, such as screws. In [14], two posts are connected together to produce a set of resonator pairs, which are utilized to achieve two passbands, one in odd mode and one in even mode. However, the design freedom of the coupling structure is limited. Moreover, the greater the coupling between two posts is, the larger the distance between the two passbands will be, but the overall distance will be limited. In comparison, a relatively large frequency ratio can be obtained by modifying the length and characteristic impedance of each transmission line of the F-shaped resonators presented in this study. Moreover, in contrast to the planar filters, the proposed filter has large design freedoms for the center frequencies and bandwidths due to the 3D filter design and the appropriate adoption of tuning elements. By using compact F-shaped resonators, the proposed filter has considerably small dimensions.

IV. CONCLUSION

A novel dual-band coaxial cavity filter is designed and fabricated in this study. By introducing F-shaped dual-mode resonators and applying tuning screws, the designed dual-band filter has large design freedoms for the center frequency

and bandwidth at both passbands. A third-order dual-band bandpass filter at 0.845 GHz/1.790 GHz with bandwidths of 12 MHz/26 MHz is designed, fabricated, and measured. The comparative measurement and simulated results demonstrate good performance, such as having lower insertion loss and more compact dimensions compared with planar dual-band bandpass filters.

REFERENCES

[1] H. Miyake, S. Kitazawa, T. Ishizaki, T. Yamada, and Y. Nagatomi, "A miniaturized monolithic dual band filter using ceramic lamination technique for dual mode portable telephones," in *Proc. IEEE Microw. Theory Technol. Soc. Int. Microw. Symp. Dig.*, 1997, pp. 789–792.

[2] S. Sun and L. Zhu, "Compact dual-band microstrip bandpass filter without external feeds," *IEEE Microw. Wireless Compon. Lett.*, vol. 15, no. 10, pp. 644–646, Oct. 2005.

[3] X.-Y. Zhang, J.-X. Chen, Q. Xue, and S.-M. Li, "Dual-band bandpass filters using stub-loaded resonators," *IEEE Microw. Wireless Compon. Lett.*, vol. 17, no. 8, pp. 583–585, Aug. 2007.

[4] G.-L. Wu, W. Mu, X.-W. Dai, and Y.-C. Jiao, "Design of novel dual-band bandpass filter with microstrip meander-loop resonator and CSRR DGS," *Prog. Electromagn. Res.*, vol. 78, pp. 17–24, 2008.

[5] X. Liu, L. P. B. Katehi, and D. Peroulis, "Novel dual-band microwave filter using dual-capacitively-loaded cavity resonators," *IEEE Microw. Wireless Compon. Lett.*, vol. 20, no. 11, pp. 610–612, Nov. 2010.

[6] J. A. Ruiz-Cruz, M. M. Fahmi, and R. R. Mansour, "Triple-conductor combline resonators for dual-band filters with enhanced guard-band selectivity," *IEEE Trans. Microw. Theory Techn.*, vol. 60, no. 12, pp. 3969–3979, Dec. 2012.

[7] J. Y. Jin, X. Q. Lin, and Q. Xue, "A novel dual-band bandpass E-plane filter using compact resonators," *IEEE Microw. Wireless Compon. Lett.*, vol. 26, no. 7, pp. 484–486, Jul. 2016.

[8] V. Nocella, L. Pelliccia, C. Tomassoni, and R. Sorrentino, "Miniaturized dual-band waveguide filter using TM dielectric-loaded dual-mode cavities," *IEEE Microw. Wireless Compon. Lett.*, vol. 26, no. 5, pp. 310–312, May 2016.

[9] E. Doumanis, L. Guan, G. Goussetis, and D. Ferling, "Dual-band bandpass double ground plane coaxial resonators and filters," *IEEE Trans. Microw. Theory Techn.*, vol. 66, no. 8, pp. 3828–3835, Aug. 2018.

[10] Z.-C. Zhang, H.-J. Li, X.-Z. Yu, Y. He, and S.-W. Wong, "Dual-narrowband/wideband filters using modified coaxial cavities with large frequency ratios," *IEEE J. Microwaves*, vol. 2, no. 4, pp. 690–698, Oct. 2022.

[11] Y. Xie, F.-C. Chen, Q.-X. Chu, and Q. Xue, "Dual-band coaxial filter and diplexer using stub-loaded resonators," *IEEE Trans. Microw. Theory Techn.*, vol. 68, no. 7, pp. 2691–2700, Jul. 2020.

[12] J.-X. Xu, M. Huang, S.-L. Song, and H.-Y. Li, "Compact multichannel filters and multiplexers based on dual-coaxial resonators," *IEEE Trans. Circuits Syst. II, Exp. Briefs*, vol. 69, no. 12, pp. 4664–4668, Dec. 2022.

[13] A. Widaa and M. Höft, "Miniaturized dual-band dual-mode TM-mode dielectric filter in planar configuration," *IEEE J. Microwaves*, vol. 2, no. 2, pp. 326–336, Apr. 2022.

[14] U. Rosenberg and S. Amari, "Novel dual-band in-line filters using coaxial dual-post resonances," in *Proc. Eur. Microw. Conf.*, 2022, pp. 48–51.

[15] L. Zhu, R. R. Mansour, and M. Yu, "A compact waveguide quasi-elliptic dual-band filter," in *Proc. IEEE Microw. Theory Technol. Soc. Int. Microw. Symp.*, 2019, pp. 1179–1182.

[16] S. Amari and M. Bekheit, "A new class of dual-mode dual-band waveguide filters," *IEEE Trans. Microw. Theory Techn.*, vol. 56, no. 8, pp. 1938–1944, Aug. 2008.

[17] M. Ohira, S. Hashimoto, Z. Ma, and X. Wang, "Coupling-matrix-based systematic design of single-DC-bias-controlled microstrip higher order tunable bandpass filters with constant absolute bandwidth and transmission zeros," *IEEE Trans. Microw. Theory Techn.*, vol. 67, no. 1, pp. 118–128, Jan. 2019.

[18] P. W. Wong and I. C. Hunter, "Electronically reconfigurable microwave bandpass filter," *IEEE Trans. Microw. Theory Techn.*, vol. 57, no. 12, pp. 3070–3079, Dec. 2009.

[19] Ansys HFSS, 2023. [Online]. Available: https://www.ansys.com/products/electronics/ansys-hfss

[20] Y. Zhan, J.-X. Chen, W. Qin, J. Li, and Z.-H. Bao, "Spurious-free differential bandpass filter using hybrid dielectric and coaxial resonators," *IEEE Microw. Wireless Compon. Lett.*, vol. 26, no. 8, pp. 574–576, Aug. 2016.